Supplementary Information (SI) for Sustainable Energy & Fuels.

Nitrogen-deficient porous g-C_3N_4 derived from HMTA-regulated supramolecular precursor for enhanced photocatalytic H_2 evolution

Liuhao Mao,[a, 1] Kailin Chen,[a, 1] Yuzhou Jiang,[a, d] Xing Kang,[a] Yazhou Zhang,*[b] Cheng Cheng,*[a] Yu Chen[c] and Jinwen Shi*[a]

[a] International Research Center for Renewable Energy (IRCRE), State Key Laboratory of Multiphase Flow in Power Engineering (MFPE), Xi'an Jiaotong University (XJTU), Xi'an 710049, China.

[b] School of Advanced Energy, IGCME, Shenzhen Campus of Sun Yat-sen University, Shenzhen 518107, China.

[c] State Key Laboratory of Electrical Insulation and Power Equipment, School of Electrical Engineering, Xi'an Jiaotong University (XJTU), Xi'an 710049, China.

[d] Huaneng Shaanxi Power Generation Co., Ltd, Xi'an 710075, China.

* Corresponding authors.
E-mail: zhangyazhou@mail.sysu.edu.cn (Yazhou Zhang); ccheng-xjtu@xjtu.edu.cn (Cheng Cheng); jinwen_shi@mail.xjtu.edu.cn (Jinwen Shi).
[1] These authors contributed equally: Liuhao Mao and Kailin Chen.

Text S1. Chemicals

Melamine ($C_3H_6N_6$), hexamethylenetetramine (HMTA, $C_6H_{12}N_4$), triethanolamine (TEOA, $C_6H_{15}NO_3$), and ethanol (C_2H_6O) were purchased from Sinopharm Chemical Reagent Co., Ltd. Chloroplatinic acid hexahydrate ($H_2PtCl_6 \cdot 6H_2O$) was purchased from Sigma-Aldrich Co., Ltd., and prepared as an aqueous solution with a Pt content of 0.8446 mg mL^{-1}. All Chemicals used were of analytical-grade without further purification. Deionized water with a resistivity of 18.25 MΩ cm was used in all experiments.

Text S2. Characterizations of samples

X-ray diffraction (XRD) patterns were recorded using a diffractometer (PANalytical X'pert MPD Pro, Netherlands) at a scan rate of 2° min^{-1} in the 2θ range of 10 to 80° under Ni-filtered Cu Kα irradiation (λ = 1.5406 Å). Fourier transform infrared (FTIR) spectra were recorded by a FTIR spectrophotometer (Bruker, Vertex 70, Germany) with using the KBr pellet technique. Brunauer–Emmette–Teller (BET) surface area measurements were conducted using a surface area and porosimetry analyzer (Micromeritics ASAP 2020, USA) with N_2 adsorption analysis, and pore volumes were calculated from the desorption branches of N_2 adsorption–desorption isotherms using the Barrett–Joyner–Halenda (BJH) method. All materials were degassed under vacuum at 423 K for 3 h. X-ray photoelectron spectroscopy (XPS) were recorded by an X-ray photoelectron spectroscope (Kratos Axis Ultra DLD, Japan) with a monochromatic Al Kα line source (hν = 1486.69 eV), with the adventitious C 1s peak at 284.8 eV used as a reference. Ultraviolet–visible (UV–vis) spectra were collected by a UV–vis–near-IR spectrophotometer (Hitachi U-4100, Japan) with a $BaSO_4$ reference in the range of 300 to 800 nm. Scanning electron microscopy (SEM) images were obtained using a field-emission scanning electron microscope (JEOL JSM-7800F, Japan). Transmission electron microscopy (TEM) images were obtained using a transmission electron microscope (FEI Tecnai G^2 F30 S-Twin, USA) with an accelerating voltage of 300 kV. Electron paramagnetic resonance (EPR) tests were performed using an EPR spectrometer (Bruker, A300-9.5/12/S/W, Germany) at room temperature in the dark. Solid-state ^{13}C nuclear magnetic resonance (NMR) spectra were acquired using an NMR spectrometer (JEOL, JNM-ECZ400R/S1, Japan). Thermogravimetric (TG) curves were recorded using a thermal analyzer (Mettler Toledo, TGA/DSC3+, Switzerland) in the range of 25 to 800°C with Ar as carrier gas. Photoluminescence (PL) spectra were obtained from a fluorescence spectrophotometer (Edinburg Instruments, FLS1000, England) at room temperature, with steady-state and time-resolved PL signals collected under excitation wavelengths of 370 and 355 nm, respectively. Element contents were obtained using an elemental analyzer (Elementar, vario MACRO cube, Italy) with He as carrier gas and O_2 as reaction gas.

Text S3. Photocatalytic performance measurements

Photocatalytic H_2-evolution measurements were carried out in a Pyrex glass reactor (50 mL), using a Xe lamp (300 W) as the light source, equipped with a 400 nm cut-off filter to provide visible-light irradiation. Photocatalyst (20 mg) was dispersed in 10% TEOA aqueous solution (40 mL), and an H_2PtCl_6 aqueous solution containing 0.6 mg Pt was subsequently added to the dispersion. The photocatalytic reactor was purged with Ar for 30 min to eliminate O_2 prior to the photocatalytic reaction. During the measurement, the solution was maintained at 35°C by circulating water and was continuously stirred. The evolved gas was detected using a North Point NP-GC-901A gas chromatograph.

Text S4. Photoelectrochemical measurements

Photoelectrochemical measurements were carried out in a three-electrode chemical cell, where the electrolyte, counter electrode, and reference electrode were Na_2SO_4 aqueous solution (0.5 M), Pt foil and Ag/AgCl, respectively. The working electrode was fabricated by depositing the sample dispersion onto a fluorine-doped tin oxide glass electrode with a load amount of 0.2 $mg \cdot cm^{-2}$. Transient photocurrent curves were recorded under chopped light irradiation at an applied voltage of +0.6 V *vs* Ag/AgCl. Electrochemical impedance spectra (EIS) were measured from 100 kHz to 1 Hz at an applied voltage of +0.6 V *vs* Ag/AgCl.

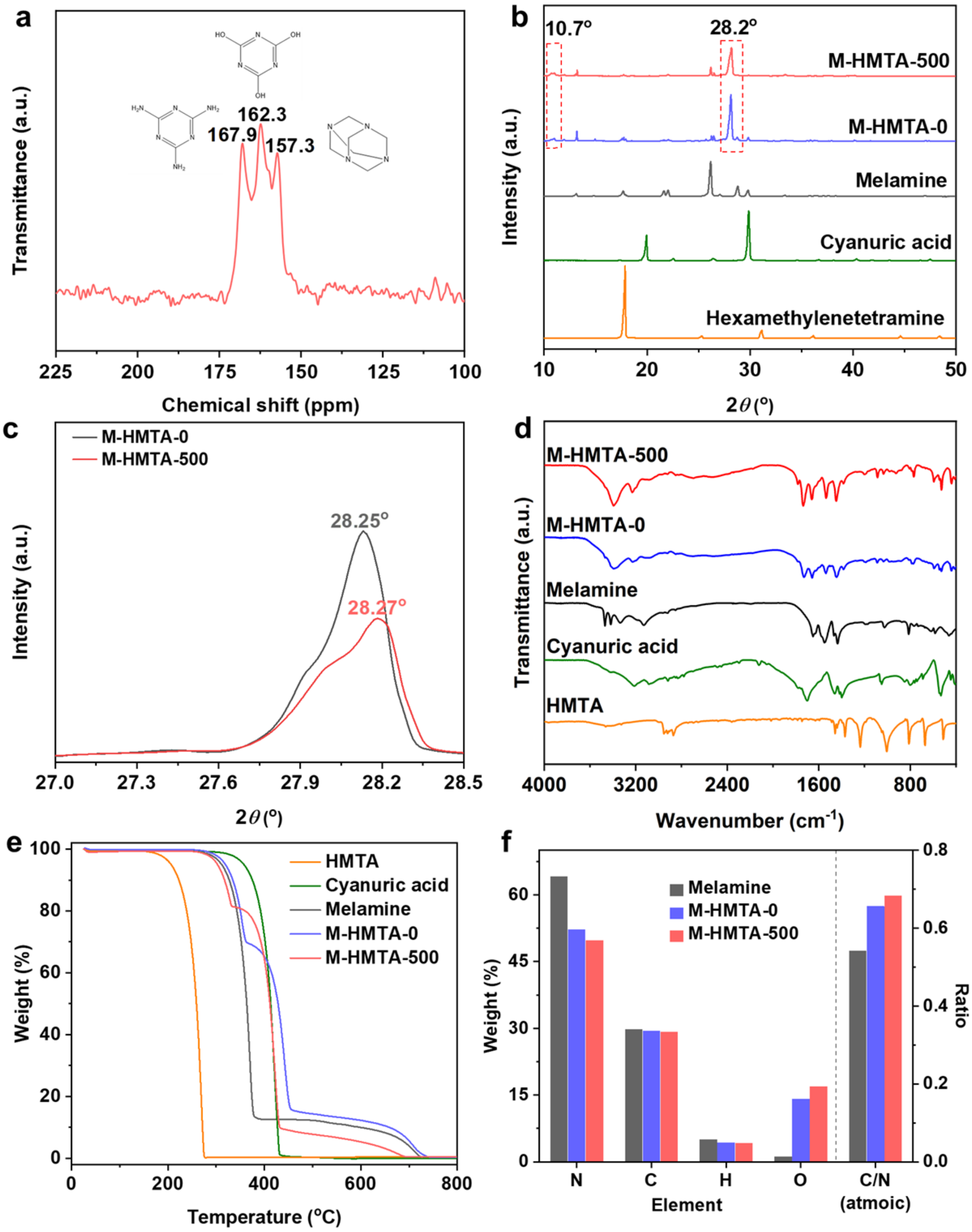

Figure S1. (a) ^{13}C NMR spectrum of M-HMTA-500, (b) XRD patterns of HMTA, cyanuric acid, melamine, M-HMTA-0 and M-HMTA-500, (c) partial magnified XRD patterns of M-HMTA-0 and M-HMTA-500 from 27.0° to 28.5°, (d) FTIR spectra and (e) TG curves of HMTA, cyanuric acid, melamine, M-HMTA-0, and M-HMTA-500, (f) elemental compositions of melamine, M-HMTA-0 and M-HMTA-500.

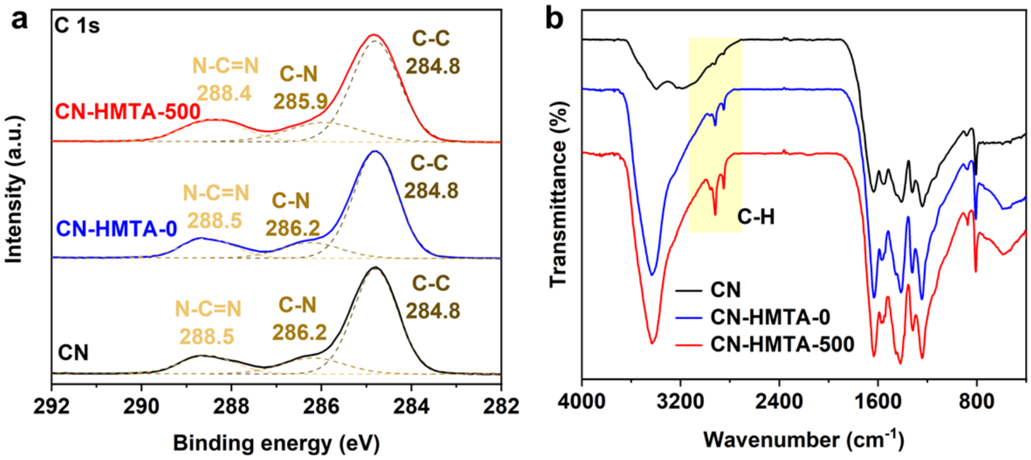

Figure S2. (a) high-resolution XPS C 1s results and (b) FTIR spectra of CN, CN-HMTA-0, and CN-HMTA-500

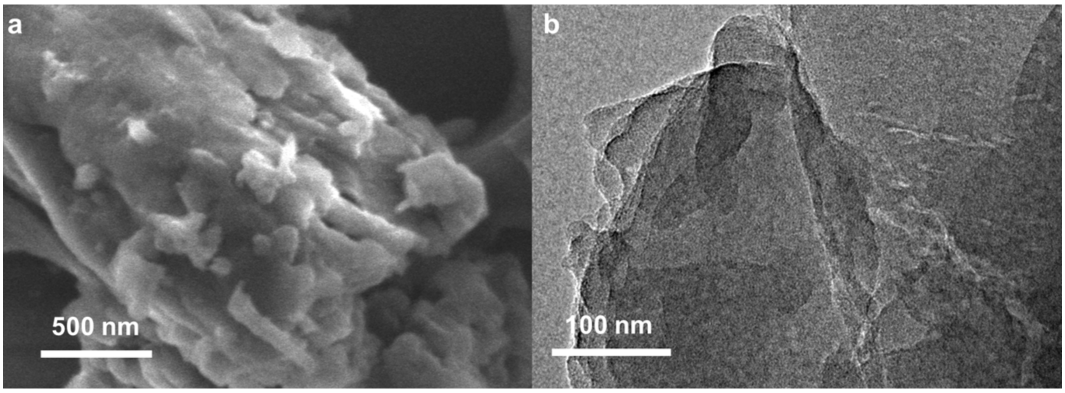

Figure S3. (a) SEM image and (b) TEM image of CN. Scale bar: 500 nm and 100 nm.

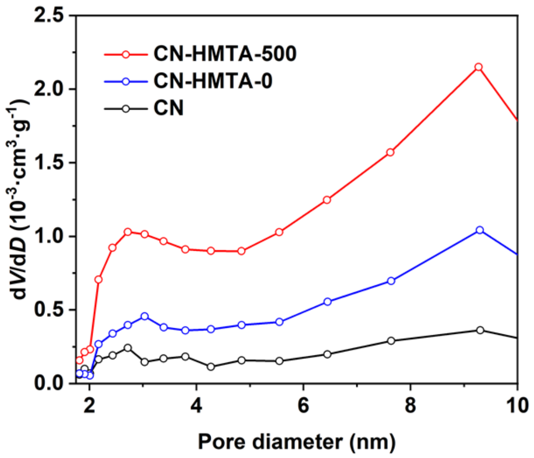

Figure S4. Partially magnified details of BJH pore-size distribution curves for CN, CN-HMTA-0, and CN-HMTA-500.

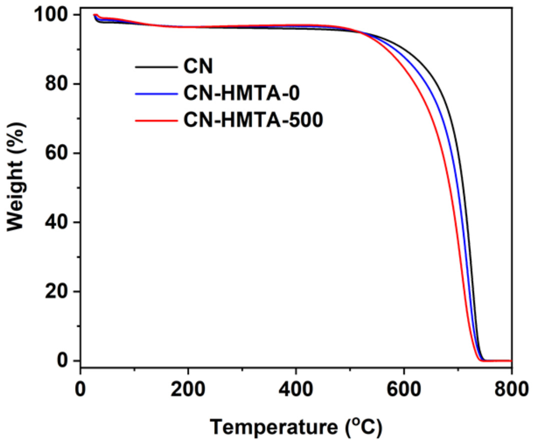

Figure S5. TG curves for CN, CN-HMTA-0, and CN-HMTA-500.

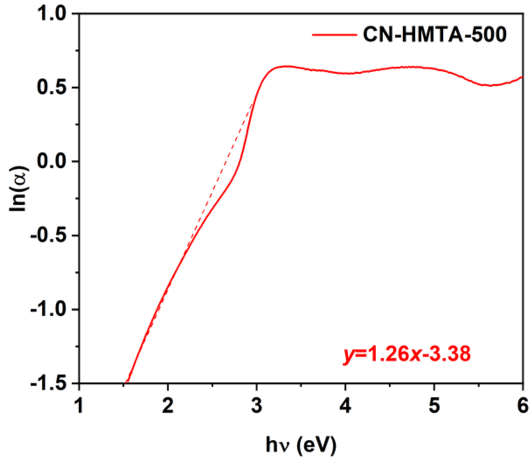

Figure S6. Urbach Plot of CN-HMTA-500.

Table S1. Binding energies of C 1s and N 1s for CN, CN-HMTA-0 and CN-HMTA-500.

Sample	C 1s			N 1s			
	C−C	C−N	N=C−N	C−N=C	N−(C)$_3$	N−H	π excitation
CN	284.8	286.2	288.5	398.5	399.5	401.0	404.2
CN-HMTA-0	284.8	286.2	288.5	398.5	399.6	401.1	404.1
CN-HMTA-500	284.8	285.9	288.4	398.4	398.8	400.5	404.2

Table S2. XRD peak intensities and corresponding ratio of CN, CN-HMTA-0 and CN-HMTA-500.

Sample	$I_{(100)}$ (CPS)	$I_{(002)}$ (CPS)	$I_{(100)}/I_{(002)}$
CN	1571	8884	0.18
CN-HMTA-0	683	5326	0.13
CN-HMTA-500	425	3532	0.12

$I_{(100)}$ and $I_{(002)}$ are intensities of XRD peaks for (100) plane and (002) plane, respectively.

Table S3. C 1s peak-area percentages (%) of different C species for CN, CN-HMTA-0 and CN-HMTA-500; N 1s peak-area percentages (%) of different N species and N 1s peak-area ratios of C−N=C to N−(C)$_3$ for CN, CN-HMTA-0 and CN-HMTA-500.

Sample	C 1s			N 1s				
	C−C	C−N	N=C−N	C−N=C	N−(C)$_3$	N−H	π excitation	C−N=C/ N−(C)$_3$
CN	69.89	15.26	14.85	51.27	30.76	8.04	9.94	1.67
CN-HMTA-0	70.54	14.15	15.31	54.83	29.29	7.32	8.56	1.87
CN-HMTA-500	63.63	18.66	17.72	30.15	39.66	24.07	6.11	0.76